

Generalized Closed-form Formulae for Feature-based Subpixel Alignment in Patch-based Matching

Laurent Valentin Jospin^{1*}, Hamid Laga², Farid Boussaid³
and Mohammed Bennamoun¹

¹School of Computer Science and Software Engineering, University of Western Australia, 35 Stirling Highway, Perth, 6009, WA, Australia.

²School of Information Technology, Murdoch University, 90 South Street, Murdoch, 6150, WA, Australia.

³School of Electrical Engineering, University of Western Australia, 35 Stirling Highway, Perth, 6009, WA, Australia.

*Corresponding author(s). E-mail(s):

laurent.jospin@research.uwa.edu.au;

Contributing authors: H.Laga@murdoch.edu.au;
farid.boussaid@uwa.edu.au; mohammed.bennamoun@uwa.edu.au;

Abstract

Patch-based matching is a technique meant to measure the disparity between pixels in a source and target image and is at the core of various methods in computer vision. When the subpixel disparity between the source and target images is required, the cost function or the target image has to be interpolated. While cost-based interpolation is easier to implement, multiple works have shown that image-based interpolation can increase the accuracy of the disparity estimate. In this paper we review closed-form formulae for subpixel disparity computation for one dimensional matching, e.g., rectified stereo matching, for the standard cost functions used in patch-based matching. We then propose new formulae to generalize to high-dimensional search spaces, which is necessary for unrectified stereo matching and optical flow. We also compare the image-based interpolation formulae with traditional cost-based formulae, and show that image-based interpolation brings a significant improvement over the cost-based interpolation methods for two dimensional search spaces, and small improvement in the case of one dimensional search spaces. The zero-mean normalized cross correlation cost function is found to be preferable for subpixel

alignment. A new error model, based on very broad assumptions is outlined in the supplementary material to demonstrate why these image-based interpolation formulas outperform their cost-based counterparts and why the zero-mean normalized cross correlation function is preferable for subpixel alignment.

Keywords: Patch-based matching, Stereo, Predictive interpolation, Subpixel

1 Introduction

The goal of image-based patch matching is to find, for a given patch in a source image I_s , the location of the same (or corresponding) patch in one or multiple target images I_t . The change in coordinates between the patch in I_s and its corresponding patch in I_t is called *disparity* and is denoted by d . Estimating the disparity d is a fundamental problem and a building block to many computer vision applications such as (multi-view) stereo vision [16, 17], optical flow estimation [43], non-rigid registration [42], velocimetry [29], photogrammetry and remote sensing [9, 45]. Although it has been extensively investigated, using either traditional methods [16] or modern deep learning-based approaches [23], achieving fine subpixel-level accurate matching remains a challenging problem.

The most generic method to achieve subpixel accuracy is to construct a continuous cost volume $C(\mathbf{p}, d)$ which measures, for every pixel \mathbf{p} and disparity value d , how well a patch centered at \mathbf{p} on the source image matches a patch located at $\mathbf{p} + d$ on the target image. Two approaches can be used to build the continuous cost volume (see Fig. 1). The continuous cost volume can be obtained by first evaluating C at discrete intervals of \mathbf{p} and d , usually at one pixel increments, and then interpolating the resulting discrete cost volume, obtaining a continuous volume from which a finer, fractional estimate of the disparity \hat{d} can be estimated (Fig. 1a). Alternatively, the interpolation can be performed in the image space where a continuous version of the cost volume is computed from a continuous version of the source and target images (Fig. 1b). In practice, the former, i.e., cost volume interpolation, is often the preferred method since it results in simple and generic closed form expressions. However, the latter, i.e., image interpolation, has been shown to result in more accurate disparity estimates than the cost volume interpolation-based methods [10, 13, 28, 34] (see Fig. 2). This is because image signals are expected to have a lower bandwidth than cost curves, therefore, they vary more slowly and are better suited for interpolation. This is a major reason why image interpolation is more effective than cost interpolation. This is explained by the Bernstein inequality in signal processing; see the Supplementary Material for more details.

Some papers have already proposed closed form solutions for image based interpolation for some specific cost functions like the Sum of Square Differences (SSD) [6, 20] or the Normalized Cross Correlation (NCC) [10, 34]. To the best of our knowledge, no work has proposed a formula for the Sum of Absolute Differences (SAD) cost function. Some of these formulae do generalize to n-dimensional patch based matching [6, 20], but only for the Sum of Square Differences (SSD) cost function.

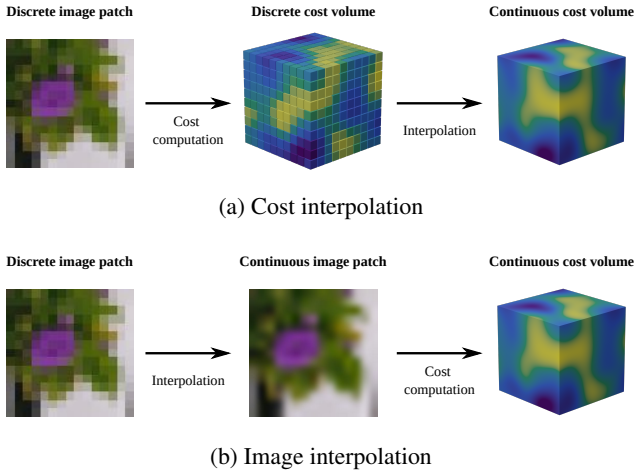


Fig. 1: In patch-based matching, two approaches can be used to achieve subpixel precision: computing the cost volume at discrete intervals and then interpolating (a) or interpolating in the image space to directly compute a continuous cost volume (b). The former approach is generally preferred for its simplicity, even though the latter is more accurate and suffer from less biases.

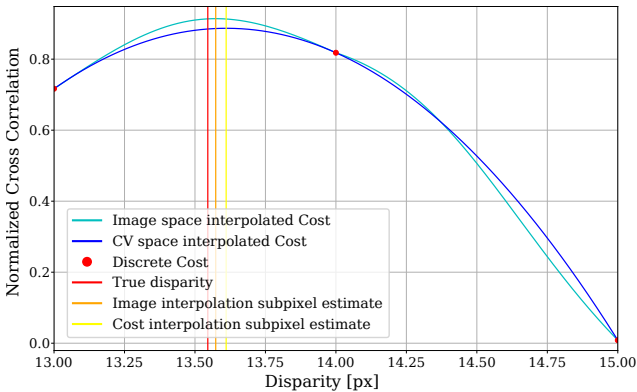


Fig. 2: Different cost curves for different cost volume interpolation methods: image space vs cost volume space (example extracted from a real image).

A generic closed form solution for image-based subpixel refinement applicable to all common cost functions and applicable to higher dimensions is still missing in the literature.

In this paper, we focus on image-based interpolation and show that closed-form formulae can be derived in a generic manner when using common dissimilarity measures such as NCC, SSD, and the SAD. Our formulation is also easy to generalize to cases where the disparity is two dimensional, like e.g., for non-rectified stereo images

4 Generalized Closed-form Formulae for Feature-based Subpixel Alignment

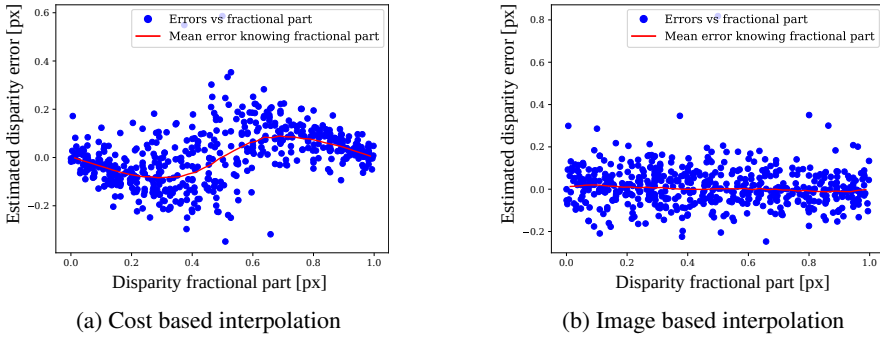


Fig. 3: The pixel-locking effect, observed in cost volume-based interpolation methods (a), occurs when the expected disparity error varies with the disparity fractional part. However, it does not occur with image-based interpolation (b).

and for optical flow estimation, and tri- or even higher-dimensional as required in applications such as medical imaging [35] or fluid dynamics [11], which are based on volumetric data [25]. The contributions of this paper are as follows;

- We propose a novel closed-form formula for image-based interpolation for 1D sub-pixel disparity refinement when using the SAD as a dissimilarity function.
- We also demonstrate that although there is no closed-form formula for the SAD for two or more dimensions, a simplex-like iterative algorithm [41] is guaranteed to lead to an exact solution in a finite number of iterations.
- We propose novel closed-form formulae for image-based interpolation for 2D, 3D and higher dimensional sub-pixel disparity refinement when using the NCC or ZNCC dissimilarity functions.
- Additionally, our formulation is generic as it can easily be adapted to new cost or score metrics. As it is formulated in tensor notation, it can also be integrated into pipelines based on tensor processing libraries (e.g., deep learning).
- We compare the subpixel accuracy of the proposed and pre-existing formulae and show that the proposed formulae, especially the ones based on ZNCC, bring a significant improvement over the cost-based methods when the search space is two dimensional, and small improvement in the case of one dimensional search spaces. The ZNCC cost function is found to yield the best estimates of all considered cost functions.
- In the supplementary material, we propose a new error model of the subpixel disparity estimation, based on very broad assumptions on the image formation model (i.e., that images are bounded and band-limited signals). This error model supports the observation we made in Section 7. It explains why these image-based interpolation formulas outperform their cost-based counterparts and why the ZNCC function is preferable for subpixel alignment.

As the underlying problem is generic for any patch-based matching model, the proposed closed-form formulae can benefit a wide range of applications. For example,

sparse patch-based matching is very important in robotics, for Simultaneous Localization and Mapping (SLAM) and related applications, where a good subpixel estimate of a reference patch position is required for a good estimate of a robot location [18]. Patch-based matching is also used in dense stereo reconstruction where a good subpixel accuracy is required to avoid visual artifacts, e.g., for augmented reality applications [30]. In addition to the traditional stereo matching methods, which are still widely adopted, especially for lightweight embedded systems [19] and remote sensing [45], the proposed formulae can benefit the modern deep learning models for stereo matching and optical flow estimation [23] which use explicit feature matching modules such as cross correlation layers [21, 26]. It can also benefit self-supervised depth estimation where (multiview) stereo images are used as supervisory signals [46].

The remainder of the paper is organized as follows; Section 2 reviews the related work. Section 3 sets the notation used throughout the paper and provides the important definitions. Section 4 derives, for various cost functions, closed form formulae for unidimensional fractional disparity reconstruction based on interpolation in the image (feature) space (Section 4.2), compared to the traditional cost based interpolation functions (Section 4.1). Section 5 discusses how the approaches presented in Section 4 can be generalized to higher dimensions. Section 6 discusses the algorithmic complexity of the different formulas and algorithms presented in the previous sections. Our experimental results, presented in Section 7, show that the proposed formulae bring an improvement in terms of accuracy over cost volume interpolation. The benefits are especially important in the case of optical flow estimation. Section 8 concludes the paper and discusses directions for future research. The Supplementary Material provides additional proofs and derivations of the formulae presented in this paper. It also provides additional discussions on the error model of the proposed formulae. We provide an open source library implementing the different formulae presented in this paper at <https://github.com/french-paragon/LibStevi>.

2 Related work

In this section, we review the different closed form solutions that have been used to achieve subpixel accuracy for disparity estimation. We classify existing closed form solutions based on whether the interpolation is done using the cost volume or the image space. We then discuss the methods for generalizing the closed form solutions to multidimensional disparity.

Cost volume interpolation. Cost volume interpolation is usually performed by fitting a parabola [7, 38], or in some cases a pair of equiangular lines forming a triangular function, around each discrete disparity value. This approach is problematic since it leads to errors that are correlated with the fractional part of the disparity due to the so called *pixel locking effect* [27, 38]. Fig. 3 illustrates the issue in more details; the mean error of the prediction is a function of the disparity fractional part. This, in turn, leads to systemic artifacts, e.g., when the disparity is used to reconstruct a 3D view of a scene in stereo vision; see Section 7.1 for more details. The mitigation

strategies proposed in the literature exploit the fact that the error caused by the pixel-locking effect is periodic, with a period of one pixel, and anti-symmetric over half that period [38]. This property can be exploited to average out the error. Since the disparity estimate for the (interpolated) image patch that is half a pixel away from the source patch should have an error that is approximately equal to minus the error of the reference patch, the initial disparity estimate can be refined by combining it with the disparity estimate of the interpolated patch (plus or minus 0.5 pixel depending in which direction this patch was interpolated). This method is efficient at removing the artifacts introduced by the pixel locking effect, but does not aim at improving the accuracy of the subpixel disparity. In practice, the method has a smoothing effect, which can also lead to some improvement. However, this smoothing effect also makes the method redundant with additional regularization that can be applied afterwards on the solution.

Image space interpolation. Image space interpolation methods lead to reconstruction errors that are decorrelated from the fractional part of the disparity. Several papers, e.g., [13, 28], have demonstrated that these methods improve subpixel accuracy since they usually lead to better estimates of the matching cost for subpixel disparities. However, these methods use exhaustive search over subpixel grids, which makes them computationally far less efficient compared to cost volume-based interpolation methods and often unsuitable for real time applications [7]. Using local optimisation methods such as iterative gradient descent [18] improves the computation time. All these methods can be made faster by using early-stopping criteria, but this will introduce quantization noise.

Different strategies have been proposed to speed up image space interpolation methods. For example, Gehrig and Franke [13] perform refinement only for small disparities. This makes sense for applications such as stereo vision where small errors in pixel coordinates lead to large errors in depth estimation only for small disparities. Mizukami et al. [28], on the other hand, use a coarse-to-fine approach where the finer disparity is computed only around each disparity.

A point that has been overlooked by those methods is that, for most of the simple image interpolation methods used in practice, closed-form formulae for the refined disparity estimators can be derived. So far, this has only been considered in the case of one dimensional disparity for the Normalized Cross Correlation (NCC) cost function [10, 34]. For the Sum of Square Differences (SSD) cost function, the formula is trivial and can be generalized to higher dimensions using a process known as predictive interpolation [6, 20]; see Section 5.2. To the best of our knowledge, no prior work solved the case of the Sum of Absolute Differences (SAD) cost function.

In this work, we propose and compare formulations for all three common cost functions and generalize them to higher dimension patch-based matching.

Multidimensionnal subpixel refinement. Multidimensional disparities received a little less attention than unidimensional disparities. The usual approach, when working in higher dimensions, is to assume that the cost function is **(1)** separable, i.e., each dimension can be refined independently of the others, and **(2)** isotropic, i.e., the separable property stays true for any orientation of the pixel coordinate system [9, 29].

Under these assumptions, any method that is applicable for unidimensional disparity generalizes to multidimensional disparities. This, however, adds a bias to the subpixel disparity estimate if the isotropy hypothesis is not respected, which is often the case in practice. Shimizu and Okutomi [39] proposed a method to jointly estimate the horizontal and vertical subpixel disparities for bi-dimensional area-based matching. The method assumes that the local subpixel optimums for each dimension, knowing all the other subpixel shifts, lie on a line. The intersection of the lines for each dimension gives the optimal multidimensional subpixel alignment. While this method can be generalized to any subpixel interpolation method, it has only been evaluated for parabola fitting. It also requires to consider a large neighborhood around the optimal position; see Section 5.1.2 for more details. Another option is to fit a multidimensional function, e.g., a paraboloid, to the cost volume [31]. This allows for more flexibility, but only applies to parabola-based cost interpolation as pyramid functions, which would generalize equiangular based refinement in one dimension, do not lead to simple closed form formulations in higher dimensions.

3 Notations and definitions

We describe in this section the notation we use throughout the paper. In particular, we adopt a tensor notation so that all patch-based matching formulae can be written using basic linear algebra expressions and are easy to translate to the tensor processing libraries that are the standards in nowadays scientific computing.

3.1 Tensor indexing and operations

Tensors are denoted with bold uppercase symbols, e.g., \mathbf{T} . The lowercase letters subscripted with a number p_1, \dots, p_n are used to index the spatial dimensions of the tensors (e.g., vertical and horizontal dimensions in images), while d_1, \dots, d_n are used to index disparity dimensions, c_1, \dots, c_n to index a channel or a feature dimension, and k_1, \dots, k_n are used for arbitrary dimensions (e.g., to refer to the other types of indices). A bold index letter without a number represents a full index, e.g., $\mathbf{k} = (k_1, \dots, k_n)$. Tensor indices are written in brackets $[\cdot]$ to distinguish them from other subscript notations, e.g., the value of channel c at pixel \mathbf{p} in the source image \mathbf{I}_s is denoted by $\mathbf{I}_{s[\mathbf{p},c]}$. The absolute value $|k_{i\mathbf{T}}|$ of a single index k_i subscripted with a tensor \mathbf{T} is used to express the size of the corresponding dimension in \mathbf{T} . $\text{Dim}_{\mathbf{T}}$ represents the number of dimensions of \mathbf{T} . A dot \cdot in place of an index indicates that all the elements on that axis are considered, e.g., $\mathbf{I}_{s[\mathbf{p},\cdot]}$ represents all channels of the source image at pixel \mathbf{p} , treated as a vector.

We write as $P_{\mathbf{W}}^l$ the patching operator with window \mathbf{W} . It is defined as:

$$(P_{\mathbf{W}}^l \mathbf{T})_{[k_1, \dots, k_l, c']} = \mathbf{T}_{[k_1 + W_{[c,1]}, \dots, k_l + W_{[c,l]}, \dots, k_n]}, \quad (1)$$

where

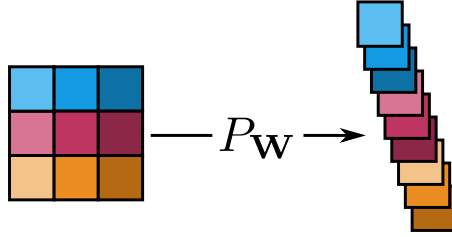


Fig. 4: Visual representation of the patching operator, when used to extract a feature vector from an image patch.

$$c'_1 = c_1 \left(\prod_{i=l+1}^n |k_{iT}| \right) + \left(\sum_{i=l+1}^{\text{Dim}T} k_i \prod_{j=l+1}^{i-1} |k_{jT}| \right)$$

and $c'_i = c_i, \forall i \neq 1$. Here, l is the number of dimensions not collapsed from the source tensor T . W is an integer tensor with the first dimensions c_1, \dots, c_m representing the output features of the operator and the last dimension of size l , where T is the target tensor, representing the index shifts from the reference index in T . Usually $l = \text{Dim}T$, but sometimes (e.g., colored images with multiple channels) it is useful to collapse one of the input tensor dimension into a feature dimension instead of indexing it. If the l argument is absent, it is then assumed that no dimension is collapsed into the features dimensions (i.e., $l = \text{Dim}T$).

3.2 Patch-based matching

Patch-based matching is the process of finding for each patch in the source image I_s , the coordinates of the corresponding patch in the target image I_t . In what follows, I without a subscript can refer to either the source or the target image. The patches are defined with a search window W , usually a square, centered at the reference pixel. In general, instead of working with the image pixels, features are used (e.g., to speed up the matching process). While many different, possibly non-linear operators, can be used to construct the features (e.g., grey-code filters kernels [3], SIFT [24], or a full convolutional network for modern deep learning architectures [15]), in this work we focus on the patching operator to get the features for the evaluation of the proposed formulae. This way, a feature volume F is given by:

$$F = P_W^l I, \quad (2)$$

with $l = 2$ for both grayscale and color images ensuring that F is always a three dimensional tensor. This formulation allows us to express the cost volume C by indexing the single dimension of the feature F instead of multiple spatial dimensions of I .

When invariance to intensity scale and constant bias is required, the feature volume needs to be whitened by subtracting the mean and scaling it so that it has a unit

variance. In what follows, \mathbf{ZF} refers to the zero-mean feature volume, \mathbf{NF} to the normalized feature volume, and \mathbf{ZNF} to the normalized zero-mean feature volume.

Various cost functions can then be computed from these feature volumes. Popular examples [16] include the cross-correlation of the normalized features, called also Normalized Cross Correlation (NCC), the Sum of Square Differences (SSD), and the Sum of Absolute Differences (SAD). Their zero mean counterparts, ZNCC, ZSSD, and ZSAD, are also popular choices. Given a disparity search range \mathbf{R} , those cost functions can be computed as:

$$NCC_{[p,d]} = \left\langle \mathbf{NF}_{s[p,\cdot]}, (P_{\mathbf{R}}\mathbf{NF}_t)_{[p,\dots,d]} \right\rangle, \quad (3)$$

$$SSD_{[p,d]} = \left\| \mathbf{F}_{s[p,\cdot]} - (P_{\mathbf{R}}\mathbf{F}_t)_{[p,\dots,d]} \right\|_2^2, \quad (4)$$

$$SAD_{[p,d]} = \left\| \mathbf{F}_{s[p,\cdot]} - (P_{\mathbf{R}}\mathbf{F}_t)_{[p,\dots,d]} \right\|_1. \quad (5)$$

The zero-mean versions of the above similarity functions can be computed by using \mathbf{NF} instead of \mathbf{F} , respectively \mathbf{ZNF} instead of \mathbf{NF} . Some papers have proposed more exotic cost options like, for example, the Median of Squares (MedS) as more robust alternative for patch based matching [20]. The MedS offers a good robustness to noise but finding the optimal solution of the Least Median of Squares (LMedS) is a non trivial combinatorial problem [14]. Existing methods addressed this issue using a variant of the RANSAC algorithm [12] to reduce the size of the search space. As such, they do not offer the speed and guarantee of the closed form solutions which can be derived for the NCC or SSD cost measures (and SAD in the one dimensional case). We included the MedS (and ZMedS) costs in our experimental comparison (Section 7), but we did not include the mathematical derivations since there was no close form solution.

In the general case, the cost function can be expressed as:

$$C_{[p,d]} = \rho \left((\mathbf{Z})(\mathbf{N})\mathbf{F}_{s[p,\cdot]}, (P_{\mathbf{R}}(\mathbf{Z})(\mathbf{N})\mathbf{F}_t)_{[p,\dots,d]} \right), \quad (6)$$

where ρ is a distance or similarity function, which takes as input two vectors from $\mathbb{R}^{|\mathcal{C}(\mathbf{Z})(\mathbf{N})\mathbf{F}_f|}$. The raw disparity $\lfloor d \rfloor$ is computed from the constructed cost volume and then refined, using some refinement formulae, to obtain a correction term $\Delta \hat{d}$ which can be added to the discrete disparity to get the final estimate of the true disparity:

$$\hat{d} = \lfloor d \rfloor + \Delta \hat{d}. \quad (7)$$

Figure 5 summarizes the generic pipeline for patch-based matching. Alternatively, the process of finding discrete matches can be implemented using an algorithm like PatchMatch [2, 22] instead of an extensive search approach to exploit the image consistency and reduce the required number of cost computations.

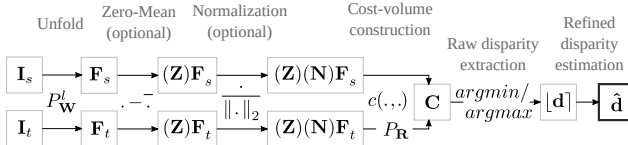


Fig. 5: Generic pipeline for local patch-based matching.

4 Subpixel interpolation formulae for unidimensional disparities

There are two main approaches to obtain $\Delta\hat{d}$: (1) interpolating from the discrete cost volume values (Section 4.1), or (2) interpolating the feature values to build a continuous cost volume (Section 4.2). In this section, we review the formulae for both approaches and derive the corresponding closed form formulae to obtain the subpixel position in the case of uni-dimensional disparities.

4.1 Cost volume-based interpolation

The two most direct methods for cost volume-based interpolation are equiangular lines-based and parabola-based [38]. For **equiangular lines-based interpolation**, $\Delta\hat{d}$ is the solution of the following equation:

$$\zeta(\Delta\hat{d} + 1) + C_{[d-1]} = -\zeta(\Delta\hat{d} - 1) + C_{[d+1]}, \quad (8)$$

with:

$$\zeta = \frac{C_{[d]} - C_{[d-1]}}{|C_{[d]} - C_{[d-1]}|} \max(|C_{[d]} - C_{[d-1]}|, |C_{[d+1]} - C_{[d]}|). \quad (9)$$

Solving this equation gives:

$$\Delta\hat{d} = \frac{C_{[d+1]} - C_{[d-1]}}{2\zeta}. \quad (10)$$

In the case of **parabola-based interpolation**, $\Delta\hat{d}$ is given by:

$$\Delta\hat{d} = \frac{C_{[d-1]} - C_{[d+1]}}{2(C_{[d+1]} - 2C_{[d]} + C_{[d-1]})}. \quad (11)$$

Alternatively, instead of a parabola, a Gaussian can be used to approximate the cost function [44]. This leads to a similar estimator as Equation (11), but using the log of the cost instead of the cost itself. Note that this makes sense only if the cost or score function has been transformed to represent a probability distribution. Otherwise, negative and zero values can lead to numerical singularities. As there is not a unique choice for such transformation, we will just ignore the Gaussian-based refinement in our comparison.

4.2 Feature space-based interpolation

Instead of using the discrete cost or score values obtained during matching, one can generate a continuous cost volume by interpolating the features. In the case of unidimensional matching, when using linear interpolation, $\Delta\hat{d}$ can be computed using closed-form formulae for all the cost functions described in Section 3. The continuous cost function is expressed as:

$$C(\mathbf{p}, \mathbf{d}) = \rho \left((N)\mathbf{F}_{s[\mathbf{p}, \cdot]}, (N)F(\mathbf{d}) \right), \quad (12)$$

where $F(\mathbf{d}) = (1 - \Delta d)(P_{\mathbf{R}}\mathbf{F}_t)_{[\mathbf{p}, \dots, [\mathbf{d}]]} + \Delta d(P_{\mathbf{R}}\mathbf{F}_t)_{[\mathbf{p}, \dots, \lceil \mathbf{d} \rceil]}$ is the interpolated target feature vector and $\Delta d = \mathbf{d} - \lfloor \mathbf{d} \rfloor$ is the subpixel adjustment.

Note that all the equations in this section are also valid when replacing F by its zero-mean version ZF . In fact, this is true for feature volumes obtained by any linear convolution operator that can be used on the images to generate the features. For the normalized versions NF and ZNF , the formulae depending on the derivative of the features with respect to the disparity need to be adapted.

In the case of normalized feature volumes, the features can be interpolated either **(a)** prior to normalization, when \mathbf{F}_s and \mathbf{F}_t are proportional to the image patches' pixels intensities, or **(b)** after normalization, when $N\mathbf{F}_s$ and $N\mathbf{F}_t$ are used for interpolation, which is done on the unit sphere. For most applications, the norm of image patches is highly spatially autocorrelated. This means that the difference between the norm of two successive patches will be similar. In this case, interpolating the features before or after normalizing them does not make a big difference. However, this is not the case for certain specific applications that deal with images with prominent high frequency features (e.g., active stereo).

The optimum subpixel correction $\Delta\hat{d}$ is reached when the derivative of the cost function with respect to Δd :

$$\frac{dC}{d\Delta d} = \left\langle \frac{\partial(N)F}{\partial\Delta d}, \nabla_{F}\rho \right\rangle, \quad (13)$$

is equals to zero. Here, $\nabla_{F}\rho$ is the gradient of the cost comparison function with respect to the (possibly normalized) features $(N)F$. $\frac{\partial(N)F}{\partial\Delta d}$ is the derivative of $(N)F$ with respect to the subpixel correction. For linear interpolation, the derivative of the features is constant in a given pixel interval:

$$\frac{\partial F(\mathbf{d})}{\partial\Delta d} = (P_{\mathbf{R}}\mathbf{F}_t)_{[\mathbf{p}, \dots, \lceil \mathbf{d} \rceil]} - (P_{\mathbf{R}}\mathbf{F}_t)_{[\mathbf{p}, \dots, [\mathbf{d}]]}. \quad (14)$$

For the normalized features, the expression becomes:

$$\frac{\partial NF}{\partial \Delta d} = \frac{\frac{\partial F(\mathbf{d})}{\partial \Delta d} \langle F(\mathbf{d}), F(\mathbf{d}) \rangle - F(\mathbf{d}) \left\langle F(\mathbf{d}), \frac{\partial F(\mathbf{d})}{\partial \Delta d} \right\rangle}{\frac{3}{\langle F(\mathbf{d}), F(\mathbf{d}) \rangle^2}}. \quad (15)$$

Note that, when setting the derivative of the cost function to 0, the denominator can be ignored as it is bounded, meaning that the different expressions derived from Equation (15) can usually be simplified.

4.2.1 Normalized Cross Correlation (NCC)

Let ρ be the cost function used to compute the cost volume C . When ρ is the normalized cross correlation then

$$\nabla_F \rho = \mathbf{F}_{s[p,\cdot]}. \quad (16)$$

Using Equation (15) to get the total derivative and setting it to zero, the formula for the optimal subpixel correction in the unidimensional disparity refinement case becomes:

$$\Delta \hat{d}_{NCC} = \frac{a_{[0,1,0]} - a_{[1,0,0]}}{a_{[0,1,0]} - a_{[0,1,1]} - a_{[1,0,0]} + a_{[1,1,0]}}, \quad (17)$$

where $a_{[\delta_0, \delta_1, \delta_2]}$ is defined as $\left\langle \mathbf{F}_{s[p,\cdot]}, (P_{\mathbf{R}} \mathbf{F}_t)_{[p,\cdot, [d] + \delta_0]} \right\rangle$ times $\left\langle (P_{\mathbf{R}} \mathbf{F}_t)_{[p,\cdot, [d] + \delta_1]}, (P_{\mathbf{R}} \mathbf{F}_t)_{[p,\cdot, [d] + \delta_2]} \right\rangle$.

While structured differently, this formula is strictly equivalent to the one presented by Psarakis et Evangelidis [34] and Delon et Rougé [10]. Psarakis et Evangelidis [34] and Delon et Rougé [10] have overlooked the important fact that using a (Z)NCC-based formula for subpixel refinement can mitigate some of the biases inherent in linear interpolation in addition to the benefits of using normalized cross-correlation (i.e., being insensitive to differences of gain or bias between the source and target images). A detailed explanation of why this is the case can be found in Section II of the Supplementary Material.

4.2.2 Sum of Square Differences (SDD)

When the cost function used to compute the cost volume is the sum of square differences, then:

$$\nabla_F \rho = 2F(\mathbf{d}) - 2\mathbf{F}_{s[p,\cdot]}. \quad (18)$$

Since the sum of square differences does not rely on normalized features, Equation (14) gives the derivative of the features. This means that the optimal

subpixel correction $\Delta\hat{d}_{SSD}$ can be computed as:

$$\Delta\hat{d}_{SSD} = \frac{\left\langle \frac{\partial F(\mathbf{d})}{\partial \Delta d}, \mathbf{F}_{s[p,\cdot]} \right\rangle}{\left\langle \frac{\partial F(\mathbf{d})}{\partial \Delta d}, \frac{\partial F(\mathbf{d})}{\partial \Delta d} \right\rangle}. \quad (19)$$

The normalized variants of SSD, NSSD and ZNSSD are strictly equivalent to NCC, respectively ZNCC [32]. This means that those variants can be treated with Equation (17).

4.2.3 Sum of Absolute Differences (SAD)

When the sum of absolute differences is used as the matching function, the gradient of the cost becomes:

$$\nabla_{F\rho} = \text{sgn}(F(\mathbf{d}) - \mathbf{F}_{s[p,\cdot]}), \quad (20)$$

which is not a regular function. However, the cost function C_{SAD} is still continuous and convex between two integer pixel disparities when the features are linearly interpolated in the interval. Its derivative is a piecewise constant function given by:

$$\frac{dC_{SAD}}{d\Delta d} = \left\langle \frac{\partial F(\mathbf{d})}{\partial \Delta d}, \text{sgn}(F(\mathbf{d}) - \mathbf{F}_{s[p,\cdot]}) \right\rangle. \quad (21)$$

The optimal subpixel correction $\Delta\hat{d}_{SAD}$ is the only point for which this derivative would be positive on one side and negative on the other. This point can be computed with a weighted median [36]:

$$\Delta\hat{d}_{SAD} = \underset{\omega}{\text{Median}} \Delta\mathring{d}, \quad (22)$$

where the potential subpixel corrections $\Delta\mathring{d}$ are given by:

$$\Delta\mathring{d}_{[c]} = \frac{\mathbf{F}_{s[p,c]} - (P_{\mathbf{R}}\mathbf{F}_t)_{[p,c,[d]]}}{(P_{\mathbf{R}}\mathbf{F}_t)_{[p,c,[d]]} - (P_{\mathbf{R}}\mathbf{F}_t)_{[p,c,[d]]}}. \quad (23)$$

The weights $\omega = \left| \frac{\partial F(\mathbf{d})}{\partial \Delta d} \right|$. Given $\Delta\mathring{d}$ and the corresponding weights ω , we have:

$$\Delta\hat{d}_{SAD} = \Delta\mathring{d}_{[\hat{c}]}, \quad (24)$$

with

$$\hat{c} = \arg \max_{c \in \mathbb{N}} 2 \sum_{i=1}^c \omega_{[i]} \leq \sum_{i=1}^{|\mathbf{c}_{\omega}|} \omega_{[i]}. \quad (25)$$

This can effectively be solved in $O(|\mathbf{c}_{\mathbf{F}}|)$ time using a median selection algorithm, which is asymptotically not worse than the complexity of the other cost functions.

5 Subpixel interpolation formulae for multidimensional disparities

The subpixel refinement formulae presented in the previous section are limited to one-dimensional patch-based matching, e.g., rectified stereo images. However, we are also interested in formulae for patch-based matching with multidimensional disparities. The multidimensional case is more general and has a wide range of applications, e.g., optical flow estimation. In what follows, Section 5.1 covers the cost volume interpolation-based formulae while Section 5.2 introduces the generalized feature volume-based formulae.

5.1 Using cost volume interpolation

Traditional cost volume-based closed-form formulae for subpixel refinement can be roughly divided into two categories: those that assume that the cost function is locally well approximated by an isotropic peak and those that assume the cost function is locally well approximated by a possibly anisotropic peak.

5.1.1 Isotropic interpolation

If the peak of the cost function is isotropic then the problem of subpixel refinement becomes separable and can be carried out independently on each dimension using any of the formulae presented in Section 4.1 [9, 29]:

$$\Delta \hat{\mathbf{d}} = \begin{pmatrix} \Delta \hat{d}(C_{[d_0-1, \dots, d_n]}, C_{[d_0, \dots, d_n]}, C_{[d_0+1, \dots, d_n]}) \\ \vdots \\ \Delta \hat{d}(C_{[d_0, \dots, d_n-1]}, C_{[d_0, \dots, d_n]}, C_{[d_0, \dots, d_n+1]}) \end{pmatrix}. \quad (26)$$

This approach has many benefits. In particular, it allows for basically any closed-form formula to be generalized to arbitrarily high dimensions. However, this baseline hypothesis, i.e., the peak of the cost function is isotropic, is not always valid, which can lead to an important bias in certain configurations [39].

5.1.2 Anisotropic interpolation

To account for possible anisotropy in the cost function peak, Shimizu and Okutomi [39] proposed a procedure where a line is fitted to the subpixel correction in one direction keeping all the other directions as constant. The optimal two-dimensional subpixel disparity then lies at the intersection of all the lines. Figure 6 gives a visual representation of the approach.

This approach has the same benefits as the separable approach presented in Section 5.1.1, i.e., it allows for basically any closed form formula to be generalized to arbitrarily high dimensions. The approach, however, has some limitations. For instance, the optimal discrete pixel adjustment for a given dimension can be different from zero if the index in the other dimension is different from zero. It means that the

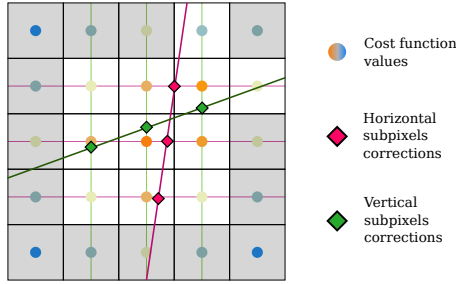


Fig. 6: Visual representation for the anisotropic cost interpolation. Pixels required for the computation are in white. The optimum is at the intersection of both lines fitting the subpixels corrections.

method might require values in the cost function arbitrarily far away from the discrete optimum. It also means that both the vertical and horizontal subpixel correction lines can be very close to being co-linear, which can lead to numerical instability. Shimizu and Okutomi [39] recommend to only consider a radius of two pixels around the discrete optimum and fall back to a default method beyond this point. Although the method can be generalized to more than two dimensions, it can quickly become impractical beyond two dimensions as the number of subpixel positions to compute grows geometrically with the number of dimensions of the disparities.

An alternative solution is to fit a multidimensional function (e.g., a paraboloid) to the data [31]. This approach seems more natural but is difficult to generalize to any formulation (e.g., for equiangular refinement).

5.2 Generalized feature volume-based refinement with barycentric and predictive interpolation

The approaches presented in Section 4.2 can be reinterpreted as solving a multidimensional optimization problem that finds $\hat{\beta}$ such that:

$$\hat{\beta} = \arg \min_{\beta} \rho(A\beta, \mathbf{f}_s), \quad (27)$$

with the additional constraints that β represents a set of barycentric coordinates, i.e., $\sum_{\beta_i \in \beta} \beta_i = 1$. \mathbf{f}_s is a reference feature vector from the source feature volume and $A = [\mathbf{f}_{t,1}, \dots, \mathbf{f}_{t,n}]$ is a matrix whose columns are the feature vectors from the target feature volume between which the interpolation is performed.

This approach can be generalized to higher dimensions as long as a closed-form formula to solve Equation (27) exists when $\dim(\beta) > 2$. In this section, we give such closed-form formula for the (Z)NCC and (Z)SSD matching functions. Unfortunately, there is no closed-form formula for the (Z)SAD matching function [40]. However, we propose an algorithm that is guaranteed to yield the correct solution in a finite number of steps.

One constraint of barycentric interpolation is that it yields a unique interpolated value for each point if and only if the interpolation domain is isomorphic to a simplex

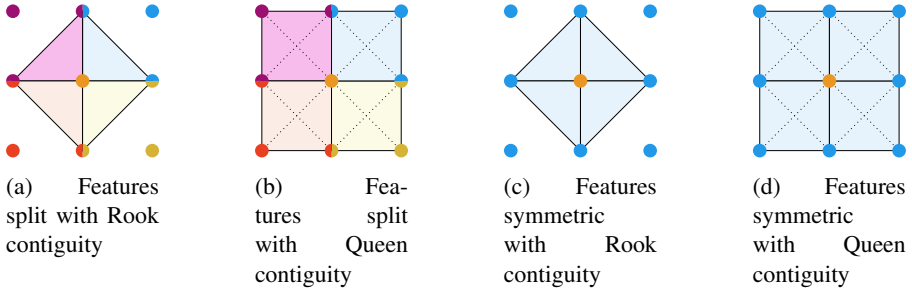


Fig. 7: The four considered approaches for 2D patch-based matching. Features are either split between the corners of the discrete match, or considered all at once. The considered features sets can be selected with either queen or rook contiguity.

(i.e., a segment in 1D, a triangle in 2D, a tetrahedron in 3D, etc.). This is, however, not the case for a pixel (for 2D refinement) nor a voxel (for 3D refinement), which have four, respectively eight, corners. Two mitigation strategies can be used; see Figure 7: **(a)** Consider only the coordinates within a given pixel or voxel for which the closest corner is the one pointed to by $\lfloor \hat{\mathbf{d}} \rfloor$. Since this set is always isomorphic to a simplex, barycentric interpolation can be used. Another benefit is that the number of considered feature vectors grows linearly instead of geometrically with the number of considered dimensions.

Alternatively, **(b)** the problem can be relaxed so that the optimal weights β are selected even if multiple weight sets lead to the same refined disparity $\hat{\mathbf{d}}$. This approach is known as predictive interpolation [6] where the interpolation weight of different image pixels is extracted from the patches themselves. This can be interpreted as interpolating the disparity in the feature space instead of interpolating the features in the disparity space. While the continuous source or target feature volumes form complex and maybe even self-intersecting hypersurfaces, it is reasonable to assume they are locally smooth. It means that, functions (e.g., the disparity) defined for each feature vector can be interpolated on said hypersurfaces.

Predictive interpolation allows to treat problems with arbitrary shapes like the four corners of a pixel, but also to generalize the approach to multiple feature vectors in lower dimensions (e.g., instead of treating the left and right pixels of $\lfloor \hat{\mathbf{d}} \rfloor$ with the equations presented in Section 4.2, both the left and the right pixels can be considered at the same time).

Another issue with barycentric interpolation is how to enforce the constraint on β . The easiest way to do it is by performing a change of variable from the barycentric coordinates β to a set of affine coordinates α :

$$M\alpha + \mathbf{f}_{t,n} = A\beta, \quad (28)$$

with $M = [\mathbf{f}_{t,1} - \mathbf{f}_{t,n}, \dots, \mathbf{f}_{t,n-1} - \mathbf{f}_{t,n}]$ and $\alpha_i = \beta_i \forall i \in [1, n-1]$.

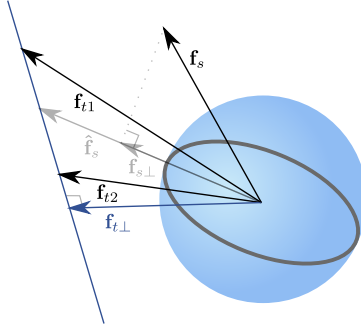


Fig. 8: Visualizing the problem of barycentric coordinate regression in the feature vector space for the NCC cost function.

The final disparity \hat{d} is computed as:

$$\hat{d} = D\hat{\beta}, \quad (29)$$

where $D = \left[[d]_{f_{t,1}}, \dots, [d]_{f_{t,n}} \right]$ is the matrix formed with the discrete disparity coordinates of the considered target features vectors.

5.2.1 Normalized Cross Correlation (NCC)

For normalized cross correlation, when more than two feature vectors are considered for interpolation, Equation (15) does not simplify to a linear function of the barycentric coefficients. However, one still can get a closed-form formula for $\hat{\beta}$ by approaching the optimization problem using geometry instead of calculus.

The optimally interpolated feature vector \hat{f}_s is the only vector in the space $\{M\alpha + f_{t,n} \mid \alpha \in \mathbb{R}^{n-1}\}$ to be co-linear with the projection $f_{s,perp}$ of f_s onto $\text{span}(A)$. This is because the normalized cross correlation is a dot product between feature vectors scaled to lie on the unit sphere. Thus, only the direction matters. Figure 8 presents visually the approach for two target feature vectors in a 3D feature space.

The procedure to compute the affine coordinates $\hat{\alpha}$ of \hat{f}_s is as follow; **First**, compute $f_{s,perp}$, which is given by:

$$f_{s,perp} = A \left(A^T A \right)^{-1} A^T f_s. \quad (30)$$

Second, find the vector $f_{t,perp}$, which is the closest vector in $\{M\alpha + f_{t,n} \mid \alpha \in \mathbb{R}^{n-1}\}$ to the origin:

$$f_{t,perp} = f_{t,n} - M \left(M^T M \right)^{-1} M^T (f_{t,n}). \quad (31)$$

Now, $\hat{\mathbf{f}}_s$ can be computed as follow:

$$\hat{\mathbf{f}}_s = \frac{\langle \mathbf{f}_{t\perp}, \mathbf{f}_{t\perp} \rangle}{\langle \mathbf{f}_{t\perp}, \mathbf{f}_{s\perp} \rangle} \mathbf{f}_{s\perp}. \quad (32)$$

Finally, $\hat{\alpha}$ can be computed as:

$$\hat{\alpha} = \left(M^\top M \right)^{-1} M^\top \left(\hat{\mathbf{f}}_s - \mathbf{f}_{t,n} \right). \quad (33)$$

Note that using least squares is not required here since we know that $\hat{\mathbf{f}}_s \in \{M\alpha + \mathbf{f}_{t,n} \mid \alpha \in \mathbb{R}^{n-1}\}$. However, it is convenient since either $\left(M^\top M \right)^{-1} M^\top$ or the QR factorization of M has already been computed to get $\mathbf{f}_{t\perp}$.

This approach is equivalent to Equation (17) when using only two target feature vectors. The proof, which we generated using the computer algebra system Maxima [8], is provided in the Supplementary Material.

5.2.2 Sum of Square Differences (SAD)

For the sum of square differences, the formula given in Equation (19) generalizes directly for any set of vectors used for the barycentric composition. We just have to replace $\frac{\partial F(\mathbf{d})}{\partial \Delta d}$ by M to get $\hat{\alpha}$, and obtain:

$$\hat{\alpha} = \left(M^\top M \right)^{-1} M^\top \left(\mathbf{f}_s - \mathbf{f}_{t,n} \right). \quad (34)$$

This formula is equivalent to the one developed in [6] and [20] for predictive interpolation.

5.2.3 Sum of Absolute Differences

In the case of a barycentric composition with more than two target vectors, finding $\hat{\alpha}$ is a least absolute difference problem of the form:

$$\hat{\alpha} = \arg \min_{\alpha} \left\| \left(\mathbf{f}_s - \mathbf{f}_{t,n} \right) - M\alpha \right\|_1. \quad (35)$$

This problem can be transformed to a linear program. Thus, one can solve it using a variant of the simplex algorithm [5]. However, this is unnecessarily complicated and suboptimal in practice, as this general method ignores much of the specificities of the least absolute difference problem. Instead, one can use gradient descent methods, which are guaranteed to reach the exact solution since the problem is convex. Dedicated variants of the algorithm, see for example [40], are guaranteed to reach the exact solution in a finite number of steps.

The gradient of the cost with respect to α is given by:

$$\nabla_{\alpha}\rho = \mathbf{M}^{\top}\nabla_{\mathbf{f}}\rho, \quad (36)$$

with $\nabla_{\mathbf{f}}\rho$ given by:

$$\nabla_{\mathbf{f}}\rho = \text{sgn}((\mathbf{f}_s - \mathbf{f}_{t,n}) - \mathbf{M}\alpha). \quad (37)$$

Starting from an initial guess $\hat{\alpha}_0$, the problem can be reduced to a uni-dimensional ℓ_1 minimization along the direction of the gradient. Starting from the new estimate, the procedure iterates until it reaches $\hat{\alpha}$. When the solution lies on the inflexion hyperplane of one of the absolute value components of the cost, some artifacts can occur since the gradient cannot be computed by a linear composition of partial derivatives. Each intermediate line-restricted optimum $\hat{\alpha}_i$ will be at the intersection of such hyperplanes. The solution is to constrain the optimization to the hyperplanes encountered in the previous optimization until the restricted space is uni-dimensional. When this occurs, the newly intersected hyperplane has to be added to the constraints and one previous hyperplane has to be deselected. The left and right gradients can be computed for each selected hyperplane. The hyperplane leading to the steepest descent when unselected is the one to remove from the constraints. As the method will end up following the edges of the cost function and will always lead to a smaller value, it is guaranteed to converge in a finite time.

The perpendicular vectors of the hyperplanes currently selected as constraints are the corresponding rows of the matrix \mathbf{M} and can be stored in a matrix \mathbf{Z} . The direction of the projected gradient is then given by:

$$\nabla_{\alpha,\mathbf{Z}}\rho = \nabla_{\alpha}\rho - \mathbf{Z}^{\top}(\mathbf{Z}\mathbf{Z}^{\top})^{-1}\mathbf{Z}\nabla_{\alpha}\rho. \quad (38)$$

Note that once a sufficient number of constraints are selected such that the space they span is unidimensional, the gradient is computed not to decide in which direction to optimize (this is given by the constraints) but to determine which constraint needs to be deselected. It also gives the direction \mathbf{d} of the parametric line $\alpha(t) = \mathbf{d}t$ along which the optimization is performed.

To compute the optimal \hat{t}_i given the optimization direction \mathbf{d}_i , the weighed median formula presented in Section 4.2.3 can be used. The potential scaling parameters $\Delta\hat{t}_i$ are given by:

$$\Delta\hat{t}_{i,[c]} = \frac{\mathbf{f}_{s,[c]} - \mathbf{f}_{t,n,[c]} - \mathbf{M}\alpha_{i,[c]}}{\mathbf{M}\mathbf{d}_{i,[c]}} \quad (39)$$

and the weights ω_i are equal to $|\mathbf{M}\mathbf{d}_{i,[c]}|$. This leads to the following iterative formula for the $\hat{\alpha}_i$:

$$\hat{\alpha}_{i+1} = \hat{\alpha}_i + \mathbf{d}_i \left(\text{Median}_{\omega_i} \Delta\hat{t}_{i,[c]} \right). \quad (40)$$

6 Algorithmic complexity of the proposed formulas

Discrete dense patch-based matching has a running complexity of $\mathcal{O}(S \times R \times F)$, with S the size of the images, R the size of the search range, and F the length of the feature vectors. While R usually represents a full dense search space, specific methods such as PatchMatch [2], and its potential improvements like Coherency Sensitive Hashing [22], can be used to reduce its size. However, in the best case, the running time complexity of dense patch-base matching would still be $\mathcal{O}(S \times F)$. For comparison, cost-based interpolation formulas have a running time complexity, when processing a whole image, of $\mathcal{O}(S)$. Image-based interpolation formulas, on the other hand, have a running time complexity of $\mathcal{O}(S \times F)$, which is slightly worse than cost-based methods but does not increase the complexity of the dense patch-base matching pipeline. The algorithm proposed in Section 5.2.2, on the other hand, is a variant of the simplex method and as such has a worst time complexity of $\mathcal{O}(S \times 2^F)$, which would increase the overall complexity of the dense patch-base matching problem. However, in practice, this is hardly an issue since, on average, the simplex still has a polynomial time complexity [41]. Also, since our method also works as a gradient descent method, it can be restarted for early iterations to speed up convergence by not following the edges of the function.

7 Experimental results

In this section, we analyze the subpixel accuracy and resistance to the pixel locking effect of the proposed closed-form formulae for subpixel refinement. We first consider the case of rectified stereo pair matching (Section 7.1), which is a one-dimensional patch-based problem. Then, in Section 7.2, we consider the problem of optical flow estimation, which is a two-dimensional patch-based matching problem. All results are provided when the interpolation of the feature volumes is performed before feature whitening. The Supplementary Material provides additional results including the case when the interpolation is performed after feature whitening.

7.1 One dimensional patch-based matching

We first evaluate the proposed formulae for one dimensional subpixel refinement. To this end, we use the 2014 Middlebury stereo dataset [37], which contains 10 high-resolution real image pairs with their corresponding very high-quality ground truth. This high quality ground truth is why we choose this dataset for evaluating subpixel refinement methods on real data. In 2021 the authors of the Middlebury 2014 datasets added 24 images pairs from 11 scenes using a subset of the pipeline of the 2014 dataset [33]. We also used the 2021 dataset for evaluation but, as it is still not as widespread in the community as the 2014 dataset, we kept the results appart and discuss them in the supplementary material. We evaluate the proposed formulae for each matching function ((Z)NCC, (Z)SSD, (Z)SAD). For comparison, we also evaluate the approximation algorithm for the MedS cost function [20]. We evaluate when interpolating separately to the left and to the right (using the barycentric interpolation approach presented in Section 4.2), and then when considering both the left and right

C	W	Mean MAE over Middlebury 2014 [px]						Mean SNR over Middlebury 2014 [dB]				
		Raw	Parabola	Equiangular	[38]	Barycentric	Predictive	Parabola	Equiangular	[38]	Barycentric	Predictive
NCC	5x5	0.261	0.150	0.154	0.146	0.134	0.155	-13.939	-27.212	-21.405	-22.113	-15.398
	7x7	0.275	0.149	0.149	0.146	0.141	0.154	-15.852	-25.014	-23.900	-25.847	-16.501
	9x9	0.281	0.153	0.151	0.150	0.151	0.158	-17.799	-23.675	-24.934	-23.897	-17.903
	11x11	0.287	0.159	0.157	0.157	0.163	0.165	-19.964	-22.847	-25.579	-22.601	-19.376
ZNCC	5x5	0.258	0.150	0.154	0.152	0.124	0.151	-13.071	-26.422	-21.270	-25.731	-15.162
	7x7	0.272	0.148	0.148	0.149	0.131	0.150	-14.909	-25.697	-23.109	-26.538	-16.362
	9x9	0.279	0.151	0.150	0.151	0.141	0.153	-16.987	-24.025	-24.370	-24.510	-17.625
	11x11	0.285	0.157	0.156	0.157	0.154	0.160	-19.225	-23.065	-25.228	-22.818	-18.832
SSD	5x5	0.281	0.176	0.180	0.180	0.164	0.195	-18.349	-25.940	-23.960	-23.436	-15.184
	7x7	0.287	0.174	0.175	0.178	0.166	0.192	-18.992	-25.365	-24.837	-24.403	-16.428
	9x9	0.291	0.176	0.176	0.179	0.172	0.192	-20.393	-23.994	-24.835	-23.404	-17.534
	11x11	0.295	0.180	0.180	0.182	0.181	0.194	-21.550	-22.601	-24.437	-22.104	-18.303
ZSSD	5x5	0.261	0.151	0.154	0.146	0.133	0.154	-13.952	-27.523	-21.457	-23.373	-15.782
	7x7	0.275	0.150	0.149	0.147	0.140	0.154	-15.933	-24.891	-23.852	-25.477	-17.002
	9x9	0.281	0.154	0.152	0.151	0.151	0.159	-17.875	-23.899	-24.907	-23.400	-18.469
	11x11	0.287	0.160	0.159	0.158	0.164	0.166	-20.041	-22.977	-25.697	-21.939	-20.009
SAD	5x5	0.285	0.183	0.176	0.180	0.184	0.215	-15.656	-21.922	-23.128	-22.782	-17.339
	7x7	0.290	0.179	0.171	0.178	0.188	0.215	-16.102	-23.013	-23.503	-23.686	-18.712
	9x9	0.293	0.178	0.170	0.178	0.191	0.215	-17.326	-24.397	-23.633	-24.706	-19.520
	11x11	0.296	0.180	0.173	0.180	0.197	0.216	-18.826	-23.666	-23.549	-23.720	-19.980
ZSAD	5x5	0.261	0.154	0.146	0.144	0.142	0.163	-9.745	-17.072	-20.151	-20.638	-17.544
	7x7	0.273	0.153	0.142	0.142	0.146	0.159	-11.180	-21.221	-22.172	-24.193	-18.183
	9x9	0.279	0.155	0.143	0.145	0.154	0.160	-12.909	-24.687	-23.805	-25.771	-19.401
	11x11	0.284	0.158	0.148	0.150	0.163	0.165	-14.805	-26.235	-24.802	-24.200	-21.112
MedS	5x5	0.298	0.203	0.202	0.204	0.271	0.369	-15.837	-18.716	-19.567	-14.745	-21.520
	7x7	0.299	0.193	0.190	0.196	0.277	0.382	-17.047	-20.702	-21.334	-15.588	-21.335
	9x9	0.303	0.191	0.189	0.195	0.284	0.390	-18.201	-22.610	-23.126	-15.563	-20.510
	11x11	0.296	0.183	0.182	0.186	0.276	0.382	-19.083	-22.042	-24.200	-14.202	-19.712
ZMedS	5x5	0.247	0.160	0.163	0.157	0.217	0.323	-10.666	-17.495	-19.572	-9.159	-18.431
	7x7	0.272	0.159	0.154	0.152	0.239	0.347	-12.508	-22.893	-22.501	-9.976	-17.241
	9x9	0.303	0.191	0.189	0.195	0.284	0.390	-14.439	-25.618	-23.962	-10.359	-16.753
	11x11	0.282	0.158	0.152	0.151	0.252	0.360	-17.130	-23.916	-25.326	-11.025	-16.622

Table 1: Aggregate results of studied formulae for the Middlebury stereo dataset (1D patch-based matching) for different correlation windows and cost functions. The best performing formula per row for a given metric is bold and the best performing formula overall is in green.

feature vectors at once (using predictive interpolation as proposed in Section 5.2). We compare against the traditional equiangular (Eq. (10)) and parabola (Eq. (11)) formulae, as well as against the formula proposed by Shimizu and Okutomi [38] to cancel the pixel locking effect of parabola-based refinement. We performed the experiment for four different correlation window sizes, namely 5×5 , 7×7 , 9×9 and 11×11 .

We first compute the raw disparity map $[d]$ using the same cost or score function as the one used for feature space refinement. We then evaluate the proposed formulae on the pixels that have been successfully matched by the previous step, hereinafter referred to as inliers. As a result, we can measure the actual subpixel accuracy of the refinement formulae rather than the initial matching algorithm's performance, since mismatched pixels would otherwise dominate the error metrics. We report in Table 1 the Mean Absolute Error (MAE) between the ground truth disparity \check{d} and the refined disparity \hat{d} . It is defined as:

$$MAE = \frac{1}{|P_{matched}|} \sum_{p \in P_{matched}} |\hat{d}_{[p]} - \check{d}_{[p]}|. \quad (41)$$

In addition to these results, which are aggregated over the entire data set, we provide in the Supplementary Material the MAE and the Root Mean Square Error (RMSE) computed on each individual image.

We also evaluated how much each method is impacted by the pixel locking effect. To this end, we use the Signal-to-Noise Ratio (SNR) where the signal under consideration $\epsilon(i)$ is the expected subpixel alignment error knowing the disparity fractional part minus the expected subpixel alignment error. It is defined as:

$$\epsilon(i) = E_{\hat{d}_i || \lfloor d_i \rfloor - \check{d}_i} [\hat{d}_i - \check{d}_i] - E_{\hat{d}} [\hat{d} - \check{d}]. \quad (42)$$

The SNR can then be computed as:

$$SNR = \frac{\sum_{i \in M} \epsilon(i)^2}{\sum_{i \in M} (\hat{d}_i - \check{d}_i - \epsilon(i))^2}. \quad (43)$$

In practice, $E_{\hat{d}_i || \lfloor d_i \rfloor - \check{d}_i} [\hat{d}_i - \check{d}_i]$ is approximated by computing the mean subpixel error in discrete intervals of disparity fractional parts; see Fig. 3. We use bins of size 1/40 pixels, which is a good compromise between precision and statistical significance.

Note that unlike signal reconstruction applications, where a higher SNR means better performance, here the SNR should be as low as possible, meaning the subpixel alignment error cannot be predicted by knowing the fractional part of the disparity.

7.1.1 Accuracy of subpixel refinement

The results of our experiment, reported in Table 1, show a clear benefit of the feature space interpolation formula when using Barycentric interpolation, as the peak performance obtained with this approach (a MAE of 0.124px) is way better than the peak performance of any other approach. Especially the additional uncertainty brought by the larger number of feature vectors considered is too detrimental when using predictive interpolation.

One important point to notice is that the proposed formulae seem to be much more impacted by the size of the correlation windows than the cost-volume based formulae. When using the NCC cost function and a large correlation window (9×9 and above), the method of Shimizu and Okutomi [38] has superior performances. The results in Table 1 indicate that other cost functions follow a similar trend. This is probably due to the fact that the disparities within the correlation window are not uniform, creating misalignment within the patches when they are matched [4]. This is, however, not an issue for cost function-based interpolation methods since the generated noise will be symmetric on each side of the optimum subpixel position, just like the parabola or equiangular kernel. For feature-based refinement, this will pose a problem, which will become more and more visible as the size of the correlation window, and thus the discrepancies between pixels disparities in the window, increases.

Note that feature-based interpolation is not suitable for the SAD cost function, with the equiangular cost-based refinement formula outperforming all alternative formulae for this cost function. However, the performance of any combination of method and correlation windows on SAD is still far from the best performing combination.



(a) Original image from the Middlebury dataset.



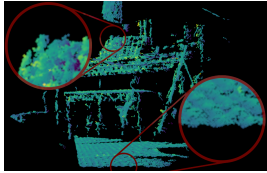
(b) Ground truth point cloud for inliers (sideview).



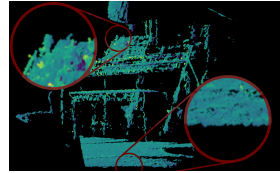
(c) Parabola cost based refined point cloud (sideview).



(d) Feature based refined point cloud (sideview).



(e) Parabola cost based refined disparity error (sideview).



(f) Feature based refined disparity error (sideview).

Fig. 9: The benefits of reducing the pixel locking effect: when refining with the parabola based formula, waves can be seen when looking at the 3D point cloud reconstructed from the disparity map when seen from the side (c). The effect is far less pronounced when using feature based refinement (d). Here showcased on the piano image from the Middlebury 2014 stereo dataset.

The results of Kim and Kak's [20] image interpolation for MedS and ZMedS costs are very poor, but remember that their iterative algorithm [20] with which we are comparing our formulas is an approximation. These two cost functions also performed relatively poorly for the cost interpolation-based methods compared to other cost functions. This is probably because the pixel with the median square error is likely to be a different pixel for different neighboring image patches, causing additional noise even when interpolating in the cost space.

The absolute best formula is a feature-based interpolation using a 5×5 correlation window and ZNCC cost function. As a matter of fact, the feature-based interpolation with the ZNCC cost function is the most effective for all correlation window sizes except 11×11 , for which the SAD with equiangular cost refinement provides the best result. In general, using a smaller correlation window is often not desirable for discrete matching. However, one can use different window sizes for the matching and refinement, since the refinement process is a local process and as such it should not be adversely impacted by ambiguous image patches elsewhere in the image.

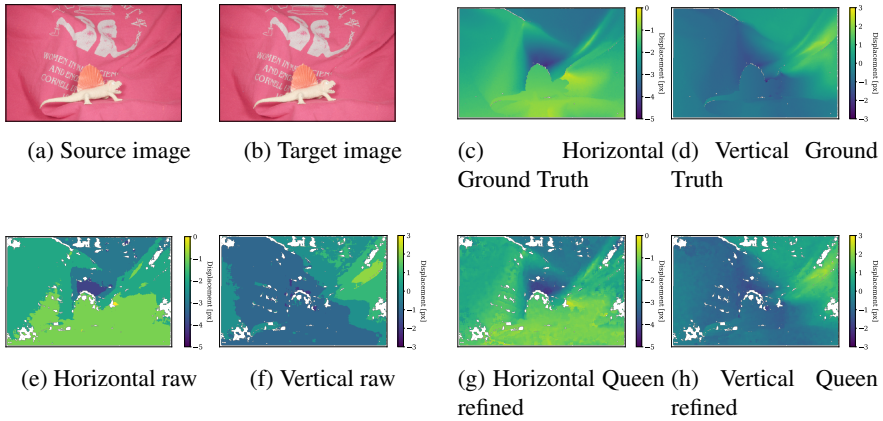


Fig. 10: Visual results of the Queen contiguity feature based refinement formula on the dimetrodon image from the Middlebury optical flow dataset.

7.1.2 Robustness to the pixel-locking effect

In terms of sensitivity to the pixel-locking effect, the parabola-based interpolation formula shows an SNR up to one order of magnitude worse than alternative methods with clearly visible artifacts in the point clouds and depth maps reconstructed from the disparity; see Figure 9. The three remaining formulae all have decent performances that are quite similar to one another. This shows that, in almost all cases, parabola cost interpolation should be avoided. The equiangular cost-based interpolation formula or Shimizu and Okutomi [38] cancellation method can always replace their parabola counterpart with minimal performance loss and no overhead in terms of computation time. Feature-based interpolation, while slightly more expensive in terms of computation time, offers good benefits in terms of reconstruction accuracy as well as robustness to the pixel-locking effect.

7.2 Two dimensional patch-based matching

To test the proposed formulae for 2D subpixel refinement, we use the optical flow Middlebury dataset, a collection of three real and seven simulated image pairs with very high quality optical flow ground truth [1]. We evaluate, for each matching function ((Z)NCC, (Z)SSD, (Z)SAD), the proposed formulae using both the Rook (Fig. 7a) and Queen (Fig. 7b) contiguity. We first consider the case where each four corners of $\lfloor d \rfloor$ are considered individually, using barycentric interpolation for the Rook contiguity (Fig. 7a) and predictive interpolation for the Queen contiguity (Fig. 7b). Then, we consider the case where each four corners of $\lfloor d \rfloor$ are considered all at the same time, using predictive interpolation in all cases (Fig. 7c and 7d). We compare against the traditional separable formula (Eq. 26) for parabola an equiangular cost interpolation, as well as against the anisotropic formula of Shimizu and Okutomi [39], again both with parabola and equiangular cost and paraboloid fitting (using least squares).

		Mean distance over Middlebury optical flow dataset [px]										
C	W	Isotropic			Anisotropic			Features split			Features symmetric	
		Raw	Parabola	Equiangular	Parabola	Equiangular	Paraboloid	Rook	Queen	Rook	Queen	
NCC	5x5	0.359	0.258	0.279	0.343	0.345	0.337	0.197	0.196	0.224	0.284	
	7x7	0.364	0.238	0.254	0.303	0.304	0.288	0.184	0.172	0.205	0.244	
	9x9	0.366	0.229	0.241	0.280	0.280	0.259	0.179	0.163	0.198	0.227	
	11x11	0.368	0.224	0.235	0.267	0.267	0.243	0.177	0.160	0.196	0.220	
ZNCC	5x5	0.358	0.255	0.276	0.342	0.344	0.331	0.194	0.194	0.226	0.287	
	7x7	0.363	0.236	0.251	0.300	0.301	0.281	0.180	0.171	0.206	0.245	
	9x9	0.365	0.226	0.239	0.278	0.278	0.254	0.175	0.162	0.198	0.227	
	11x11	0.366	0.221	0.232	0.265	0.265	0.238	0.174	0.159	0.196	0.219	
SSD	5x5	0.365	0.263	0.284	0.343	0.345	0.334	0.201	0.200	0.227	0.282	
	7x7	0.366	0.242	0.258	0.304	0.305	0.286	0.186	0.176	0.207	0.244	
	9x9	0.367	0.231	0.244	0.281	0.282	0.259	0.180	0.166	0.199	0.228	
	11x11	0.368	0.226	0.237	0.268	0.268	0.242	0.178	0.163	0.197	0.220	
ZSSD	5x5	0.359	0.257	0.277	0.342	0.344	0.335	0.236	0.234	0.264	0.323	
	7x7	0.363	0.237	0.252	0.301	0.302	0.285	0.206	0.194	0.228	0.265	
	9x9	0.365	0.227	0.240	0.278	0.279	0.257	0.193	0.178	0.213	0.241	
	11x11	0.366	0.223	0.233	0.265	0.265	0.241	0.189	0.173	0.208	0.231	
SAD	5x5	0.365	0.265	0.270	0.345	0.344	0.304	0.211	0.208	0.237	0.291	
	7x7	0.366	0.248	0.245	0.303	0.301	0.261	0.192	0.181	0.212	0.248	
	9x9	0.365	0.239	0.232	0.279	0.275	0.237	0.183	0.167	0.200	0.227	
	11x11	0.365	0.234	0.224	0.264	0.259	0.224	0.178	0.161	0.194	0.215	
ZSAD	5x5	0.359	0.260	0.264	0.346	0.345	0.305	0.245	0.243	0.275	0.333	
	7x7	0.363	0.245	0.241	0.304	0.301	0.261	0.209	0.197	0.232	0.269	
	9x9	0.364	0.237	0.229	0.280	0.276	0.237	0.195	0.179	0.214	0.241	
	11x11	0.365	0.233	0.223	0.265	0.261	0.224	0.188	0.170	0.205	0.226	
MedS	5x5	0.365	0.298	0.333	0.400	0.407	0.367	0.342	0.353	0.363	0.369	
	7x7	0.368	0.274	0.303	0.355	0.364	0.321	0.337	0.348	0.362	0.366	
	9x9	0.367	0.260	0.285	0.327	0.335	0.291	0.333	0.345	0.360	0.364	
	11x11	0.365	0.251	0.273	0.307	0.315	0.271	0.331	0.343	0.359	0.362	
ZMedS	5x5	0.360	0.289	0.305	0.396	0.395	0.362	0.330	0.341	0.356	0.363	
	7x7	0.369	0.270	0.277	0.351	0.348	0.315	0.331	0.342	0.361	0.366	
	9x9	0.371	0.259	0.260	0.322	0.319	0.285	0.330	0.342	0.362	0.367	
	11x11	0.371	0.252	0.250	0.303	0.299	0.266	0.330	0.342	0.362	0.367	

Table 2: Aggregate results of the studied formulae for the Middlebury optical flow dataset (2D patch-based matching) for different correlation windows and cost functions. The best performing formula per row is in bold and the overall best performing formula is in green.

Similar to Section 7.1, we first compute the raw disparity map using the same cost function as the one used for subpixel refinement. We then evaluate our formula on the inliers. To be consistent with the MAE , which we used in the 1D case (Section 7.1), we report the mean norm of the difference between the ground truth optical flow \hat{d} and the refined optical flow \hat{d} , denoted as MD :

$$MD = \frac{1}{|P_{matched}|} \sum_{p \in P_{matched}} \left\| \hat{d}_{[p]} - \check{d}_{[p]} \right\|_2. \quad (44)$$

We also provide, in the Supplementary Material, the MD per image.

The results, reported in Table 2, show very clear benefits for feature-based formulae, and more specifically the Queen contiguity-based formula when each corner of $[d]$ is considered independently. **In term of accuracy, the overall best performing method is once again the ZNCC based formula, but this time when using an 11×11 correlation window.** In fact, unlike the one dimensional case, the performance of almost all feature-based formulae increases with the size of the correlation window. This can be explained by multiple factors but the most important one is that

when reconstructing optical flow, as long as the relative motion between two consecutive frames is small, the search space is smaller and the risk of having large flow variations within the correlation windows is thus limited.

Visually, the improvement of the proposed feature-based refinement formula is very clear. In Figure 10, for example, one can see that most of the details invisible in the raw displacement map can be spotted on the refined map.

8 Conclusion and future work

This paper studied closed-form formulae for subpixel refinement. We proposed new and extended existing feature-based refinement formulae for any-dimensional patch-based matching. We have evaluated those formulae against existing closed-form formulae based on cost interpolation for stereo matching and optical flow evaluation. Our experiments show that the proposed formulae offer clear benefits in almost all of the considered cases. In particular, our generalized two dimensional formula for the ZNCC cost function attains the absolute best performance compared to all the other tested formulas on the Middlebury optical-flow dataset. The proposed feature-based formulae can easily and directly replace their cost-based counterparts in existing machine vision and image processing applications. While the focus of this work was mostly mathematical, i.e., deriving and analyzing formulae, we plan in the future to consider practical applications by implementing the proposed formulae in more complete pipelines for applications such as stereo vision. We also plan to generalize the proposed formulae to the non-linear features used in practice, for which interpolation in the image space is no longer equivalent to interpolation in the feature space.

9 Acknowledgments

This research is supported by the Australian Research Council <https://www.arc.gov.au/> (Grant no. DP210101682).

References

- [1] Simon Baker, Daniel Scharstein, JP Lewis, Stefan Roth, Michael J Black, and Richard Szeliski. A database and evaluation methodology for optical flow. *Int. J. Comput. Vis.*, 92(1):1–31, 2011.
- [2] Connelly Barnes, Eli Shechtman, Adam Finkelstein, and Dan B Goldman. Patchmatch: A randomized correspondence algorithm for structural image editing. *ACM Trans. Graph.*, 28(3):24, 2009.
- [3] Gil Ben-Artzi, Hagit Hel-Or, and Yacov Hel-Or. The gray-code filter kernels. *IEEE Trans. Pattern Anal. Mach. Intell.*, 29(3):382–393, 2007.
- [4] Michael Bleyer, Christoph Rhemann, and Carsten Rother. Patchmatch stereo-stereo matching with slanted support windows. In *Bmvc*, volume 11, pages 1–11, 2011.
- [5] Stephen Boyd, Stephen P Boyd, and Lieven Vandenberghe. *Convex optimization*. Cambridge university press, 2004.

- [6] Hamish Bradley, Donald Bailey, Steven Le Moan, Peter Gaenz, and Sven Simon. Sub-pixel registration technique for x-ray phase contrast imaging. In *2019 International Conference on Image and Vision Computing New Zealand (IVCNZ)*, pages 1–5, 2019.
- [7] Peng Cheng and Chia-Hsiang Menq. Cancelling bias induced by correlation coefficient interpolation for sub-pixel image registration. *Measurement Science and Technology*, 24(3):035404, feb 2013.
- [8] Maxima contributors. Maxima, a computer algebra system.
- [9] Misganu Debella-Gilo and Andreas Kääh. *Sub-pixel precision image matching for displacement measurement of mass movement using normalised crosscorrelation*. na, 2010.
- [10] Julie Delon and Bernard Rougé. Small baseline stereovision. *Journal of Mathematical Imaging and Vision*, 28(3):209–223, Jul 2007.
- [11] Stefano Discetti and Tommaso Astarita. Fast 3d piv with direct sparse cross-correlations. *Exp. Fluids*, 53(5):1437–1451, Nov 2012.
- [12] Martin A. Fischler and Robert C. Bolles. Random sample consensus: A paradigm for model fitting with applications to image analysis and automated cartography. *Commun. ACM*, 24(6):381–395, jun 1981.
- [13] S. K. Gehrig and U. Franke. Improving stereo sub-pixel accuracy for long range stereo. In *2007 IEEE 11th International Conference on Computer Vision*, pages 1–7, 2007.
- [14] A Giloni and M Padberg. Least trimmed squares regression, least median squares regression, and mathematical programming. *Mathematical and Computer Modelling*, 35(9-10):1043–1060, 2002.
- [15] Xufeng Han, Thomas Leung, Yangqing Jia, Rahul Sukthankar, and Alexander C. Berg. Matchnet: Unifying feature and metric learning for patch-based matching. In *Proceedings of the IEEE Conference on Computer Vision and Pattern Recognition (CVPR)*, June 2015.
- [16] Heiko Hirschmuller and Daniel Scharstein. Evaluation of cost functions for stereo matching. In *2007 IEEE Conference on Computer Vision and Pattern Recognition*, pages 1–8, 2007.
- [17] Heiko Hirschmuller and Daniel Scharstein. Evaluation of stereo matching costs on images with radiometric differences. *IEEE Trans. Pattern Anal. Mach. Intell.*, 31(9):1582–1599, 2009.
- [18] Laurent Jospin, Alexis Stoven-Dubois, and Davide Antonio Cucci. Photometric long-range positioning of led targets for cooperative navigation in uavs. *Drones*, 3(3), 2019.
- [19] Leonid Keselman, John Iselin Woodfill, Anders Grunnet-Jepsen, and Achintya Bhowmik. Intel realsense stereoscopic depth cameras. In *Proceedings of the IEEE Conference on Computer Vision and Pattern Recognition (CVPR) Workshops*, July 2017.
- [20] Yeon-Ho Kim and A.C. Kak. Error analysis of robust optical flow estimation by least median of squares methods for the varying illumination model. *IEEE Trans. Pattern Anal. Mach. Intell.*, 28(9):1418–1435, 2006.
- [21] Patrick Knöbelreiter and Thomas Pock. Learned collaborative stereo refinement. *Int. J. Comput. Vis.*, 129(9):2565–2582, Sep 2021.

- [22] Simon Korman and Shai Avidan. Coherency sensitive hashing. *IEEE Trans. Pattern Anal. Mach. Intell.*, 38(6):1099–1112, 2016.
- [23] Hamid Laga, Laurent Valentin Jospin, Farid Boussaid, and Mohammed Benamoun. A survey on deep learning techniques for stereo-based depth estimation. *IEEE Trans. Pattern Anal. Mach. Intell.*, 2020.
- [24] D.G. Lowe. Object recognition from local scale-invariant features. In *Proceedings of the Seventh IEEE International Conference on Computer Vision*, volume 2, pages 1150–1157 vol.2, 1999.
- [25] Kecheng Lu, Chaoli Wang, Keqin Wu, Minglun Gong, and Yunhai Wang. A unified framework for exploring time-varying volumetric data based on block correspondence. *Visual Informatics*, 3(4):157–165, 2019.
- [26] W. Mao, M. Wang, J. Zhou, and M. Gong. Semi-dense stereo matching using dual CNNs. In *2019 IEEE Winter Conference on Applications of Computer Vision (WACV)*, pages 1588–1597, 2019.
- [27] V. Miclea, C. Vancea, and S. Nedevschi. New sub-pixel interpolation functions for accurate real-time stereo-matching algorithms. In *2015 IEEE International Conference on Intelligent Computer Communication and Processing (ICCP)*, pages 173–178, 2015.
- [28] Y. Mizukami, K. Okada, A. Nomura, S. Nakanishi, and K. Tadamura. Sub-pixel disparity search for binocular stereo vision. In *Proceedings of the 21st International Conference on Pattern Recognition (ICPR2012)*, pages 364–367, 2012.
- [29] H. Nobach and M. Honkanen. Two-dimensional gaussian regression for sub-pixel displacement estimation in particle image velocimetry or particle position estimation in particle tracking velocimetry. *Exp. Fluids*, 38(4):511–515, Apr 2005.
- [30] Orts-Escolano Sergio, Dou Mingsong, Tankovich Vladimir, Loop Charles, Cai Qin, Chou Philip A., Mennicken Sarah, Valentin Julien, Pradeep Vivek, Wang Shenlong, Kang Sing Bing, Rhemann Christoph, Kohli Pushmeet, Lutchn Yuliya, Keskin Cem, Izadi Shahram, Fanello Sean, Chang Wayne, Kowdle Adarsh, Degtyarev Yury, Kim David, Davidson Philip L., and Khamis Sameh. Holoportation. *Proceedings of the 29th Annual Symposium on User Interface Software and Technology*, pages 741–754, 2016.
- [31] Luca Pallotta, Gaetano Giunta, and Carmine Clemente. Subpixel sar image registration through parabolic interpolation of the 2-d cross correlation. *IEEE Trans Geosci Remote Sens*, 58(6):4132–4144, 2020.
- [32] Bing Pan, Huimin Xie, and Zhaoyang Wang. Equivalence of digital image correlation criteria for pattern matching. *Applied optics*, 49:5501–9, 10 2010.
- [33] Guanghan Pan, Tiansheng Sun, Toby Weed, Roger Dai, Kyle Meredith, Tommaso Monaco, Nick Mosier, and Daniel Scharstein. 2021 mobile stereo datasets with ground truth.
- [34] E.Z. Psarakis and G.D. Evangelidis. An enhanced correlation-based method for stereo correspondence with subpixel accuracy. In *Tenth IEEE International Conference on Computer Vision (ICCV'05) Volume 1*, volume 1, pages 907–912 Vol. 1, 2005.

- [35] J. Ruiz-Alzola, C.-F. Westin, S.K. Warfield, C. Alberola, S. Maier, and R. Kikinis. Nonrigid registration of 3d tensor medical data. *Medical Image Analysis*, 6(2):143–161, 2002.
- [36] Kristian Sabo, Rudolf Scitovski, and Ivan Vazler. Searching for a best least absolute deviations solution of an overdetermined system of linear equations motivated by searching for a best least absolute deviations hyperplane on the basis of given data. *Journal of Optimization Theory and Applications*, 149(2):293–314, May 2011.
- [37] Daniel Scharstein, Heiko Hirschmüller, York Kitajima, Greg Krathwohl, Nera Nešić, Xi Wang, and Porter Westling. High-resolution stereo datasets with subpixel-accurate ground truth. In *German conference on pattern recognition*, pages 31–42. Springer, 2014.
- [38] Masao Shimizu and Masatoshi Okutomi. Sub-pixel estimation error cancellation on area-based matching. *Int. J. Comput. Vis.*, 63(3):207–224, 2005.
- [39] Masao Shimizu and Masatoshi Okutomi. Two-dimensional simultaneous sub-pixel estimation for area-based matching. *Systems and Computers in Japan*, 36(2):1–11, 2005.
- [40] Ana Sović Kržić and Damir Seršić. L1 minimization using recursive reduction of dimensionality. *Signal Process.*, 151:119–129, 2018.
- [41] Daniel A. Spielman and Shang-Hua Teng. Smoothed analysis of algorithms: Why the simplex algorithm usually takes polynomial time. *J. ACM*, 51(3):385–463, may 2004.
- [42] Frédéric Sur, Benoît Blaysat, and Michel Grédiac. On biases in displacement estimation for image registration, with a focus on photomechanics - Extended version. Research report, LORIA (Université de Lorraine, CNRS, INRIA) ; Institut Pascal (Université Clermont-Auvergne, SIGMA, CNRS), June 2020.
- [43] Christoph Vogel, Stefan Roth, and Konrad Schindler. An evaluation of data costs for optical flow. In Joachim Weickert, Matthias Hein, and Bernt Schiele, editors, *Pattern Recognition*, pages 343–353, Berlin, Heidelberg, 2013. Springer Berlin Heidelberg.
- [44] J Westerweel. Fundamentals of digital particle image velocimetry. *Measurement Science and Technology*, 8(12):1379–1392, dec 1997.
- [45] Zhen Ye, Yusheng Xu, Hao Chen, Jingwei Zhu, Xiaohua Tong, and Uwe Stilla. Area-based dense image matching with subpixel accuracy for remote sensing applications: Practical analysis and comparative study. *Remote Sensing*, 12(4), 2020.
- [46] Yinda Zhang, Sameh Khamis, Christoph Rhemann, Julien Valentin, Adarsh Kowdle, Vladimir Tankovich, Michael Schoenberg, Shahram Izadi, Thomas Funkhouser, and Sean Fanello. Activestereonet: End-to-end self-supervised learning for active stereo systems. In *Proceedings of the European Conference on Computer Vision (ECCV)*, September 2018.